

## Dispersion measures of fast radio burst host galaxies derived from IllustrisTNG simulation

G. Q. ZHANG,<sup>1</sup> HAI YU,<sup>2</sup> J. H. HE,<sup>1,3</sup> AND F. Y. WANG<sup>1,3</sup>

<sup>1</sup>*School of Astronomy and Space Science, Nanjing University, Nanjing 210093, China*

<sup>2</sup>*Department of Astronomy, School of Physics and Astronomy, Shanghai Jiao Tong University, Shanghai, China*

<sup>3</sup>*Key Laboratory of Modern Astronomy and Astrophysics (Nanjing University), Ministry of Education, Nanjing 210093, China*

### ABSTRACT

We calculate the dispersion measures (DMs) contributed by host galaxies of fast radio bursts (FRBs). Based on a few host galaxy observations, a large sample of galaxy with similar properties to observed ones has been selected from the IllustrisTNG simulation. They are used to compute the distributions of host galaxy DMs for repeating and non-repeating FRBs. For repeating FRBs, we infer the  $DM_{\text{host}}$  for FRBs like FRB 121102 and FRB 180916 by assuming that the burst sites are tracing the star formation rates in host galaxies. The median  $DM_{\text{host}}$  are  $35(1+z)^{1.08}$  and  $96(1+z)^{0.83}$  pc cm<sup>-3</sup> for FRBs like FRB 121102 and FRB 180916, respectively. In another case, the median of  $DM_{\text{host}}$  is about 30 – 70 pc cm<sup>-3</sup> for non-repeating FRBs in the redshift range  $z = 0.1 - 1.5$ , assuming that the burst sites are the locations of binary neutron star mergers. In this case, the evolution of the median  $DM_{\text{host}}$  can be calculated by  $33(1+z)^{0.84}$  pc cm<sup>-3</sup>. The distributions of  $DM_{\text{host}}$  of repeating and non-repeating FRBs can be well fitted with the log-normal function. Our results can be used to infer redshifts of non-localized FRBs.

*Keywords:* radio continuum: transients–methods: statistical–general: galaxies

### 1. INTRODUCTION

Fast radio bursts (FRBs) are radio transients with short duration and high dispersion measures (DMs). After the first FRB was discovered (Lorimer et al. 2007), a few hundred FRBs have been observed by different telescopes to date (Thornton et al. 2013; Petroff et al. 2016; CHIME/FRB Collaboration et al. 2019a; Shannon et al. 2018). Observationally, there are two types of FRBs, repeating FRBs and non-repeating FRBs. Till now, twenty repeating FRBs have been published (Spitler et al. 2016; CHIME/FRB Collaboration et al. 2019b,c; Fonseca et al. 2020). For comparison, most FRBs are apparently non-repeating events. The data of published FRBs can be found in the FRB catalog (Petroff et al. 2016).

The physical origin of FRBs is still under debate (for recent reviews, see Platts et al. 2019; Cordes & Chatterjee 2019; Petroff et al. 2019). More recently, a radio burst from Galactic magnetar SGR

1935+2154 was discovered (The CHIME/FRB Collaboration et al. 2020; Bochenek et al. 2020), which supports the conjecture that some FRBs are produced by magnetars. The merger of compact binary is also a promising model for non-repeating FRBs, which has been discussed by many works (Totani 2013; Wang et al. 2016).

The large DMs of FRBs are well beyond the contribution from the Milky Way galaxy, which indicates an extragalactic origin. The localization of FRB 121102 (Tendulkar et al. 2017), FRB 180924 (Bannister et al. 2019), FRB 190523 (Ravi et al. 2019), FRB 181112 (Prochaska et al. 2019), and FRB 180916 (Marcote et al. 2020) support their cosmological origin. Therefore, FRBs can be used as cosmological probes, such as constraining the cosmological parameters (Gao et al. 2014; Zhou et al. 2014; Walters et al. 2018; Jaroszynski 2019; Li et al. 2018), measuring the cosmological proper distance (Yu & Wang 2017), constraining the baryon number density (Deng & Zhang 2014; Wei et al. 2019; Li et al. 2019b; Macquart et al. 2020), testing dark matter models (Muñoz et al. 2016; Wang & Wang 2018), measuring Hubble parameter (Wu et al. 2020), testing Einstein equivalent principle (Wei et al. 2015; Yu et al. 2018) and testing hydrogen and helium reionization histories (Fialkov & Loeb 2016; Caleb et al. 2019).

The main difficulty in using FRBs for cosmological purpose is how to determine their redshifts. Theoretically, the redshift of FRB can be derived from the observed DM, which is the integration of free electron number density along a given line of sight. According to their origin, the observed DM can be divided into several parts:

$$DM = DM_{\text{MW}} + DM_{\text{halo}} + DM_{\text{IGM}} + \frac{DM_{\text{host}} + DM_{\text{source}}}{1+z}, \quad (1)$$

which includes the contributions from the interstellar medium of the Milky Way ( $DM_{\text{MW}}$ ), the halo of the Milky Way ( $DM_{\text{halo}}$ ), the intergalactic medium (IGM) ( $DM_{\text{IGM}}$ ), the host galaxy ( $DM_{\text{host}}$ ) and the source ( $DM_{\text{source}}$ ).  $DM_{\text{MW}}$  can be derived from the NE2001 model (Cordes & Lazio 2002) or YMW16 model (Yao et al. 2017). We have a poor understanding of  $DM_{\text{halo}}$ . Dolag et al. (2015) found the typical value of  $DM_{\text{halo}} \sim 30 \text{ pc cm}^{-3}$  from numerical simulations. Prochaska & Zheng (2019) estimated that  $DM_{\text{halo}}$  is about  $50 \sim 80 \text{ pc cm}^{-3}$ . The relation between  $DM_{\text{IGM}}$  and redshift  $z$  has been studied by some works (Ioka 2003; Deng & Zhang 2014), which can be used to compute the pseudo redshifts of FRBs. The source contribution  $DM_{\text{source}}$  depends on the unclear central engine of FRBs. For example, if FRBs are produced by the collapses of massive stars, the values of  $DM_{\text{source}}$  are large (Piro 2016). On the other hand, if FRBs are produced by mergers of binary neutron stars (Wang et al. 2016; Zhang 2020), they have a small  $DM_{\text{source}}$  (Margalit et al. 2019; Wang et al. 2020). If the central engine is known, the value of  $DM_{\text{source}}$  can be derived analytically under some assumptions (Piro 2016; Yang & Zhang 2017; Wang et al. 2020). In our discussion, this term is ignored. The value of  $DM_{\text{host}}$  is hard to determine. For FRB 121102, Tendulkar et al. (2017) obtained the value of host galaxy DM as  $55 \leq DM_{\text{host}} \leq 225 \text{ pc cm}^{-3}$ , which may consist of large contribution from the sources. Marcote et al. (2020) estimated the  $DM_{\text{host}}$  of FRB 180916 is less than  $70 \text{ pc cm}^{-3}$ . For non-repeating FRBs, Bannister et al. (2019) found  $DM_{\text{host}} \simeq 30 - 81 \text{ pc cm}^{-3}$  for FRB 180924.

Until now, only ten FRBs have been localized, including the Galactic FRB 200428. Using Very Large Array (VLA), FRB 121102 has been localized to a dwarf galaxy with low metallicity and low star formation rate (SFR) (Chatterjee et al. 2017; Tendulkar et al. 2017). FRB 180916 is localized to a spiral galaxy with high stellar mass and SFR (Marcote et al. 2020). For non-repeating FRBs,

Ravi et al. (2019) localized the host galaxy of FRB 190523 through Deep Synoptic Array ten-antenna prototype (DSA-10). Using Australian Square Kilometer Array Pathfinder (ASKAP), the host galaxies of FRB 180924 (Bannister et al. 2019) and FRB 181112 (Prochaska et al. 2019) have also been determined. Recently, four ASKAP localized FRBs have been released (Macquart et al. 2020). The properties of these host galaxies are listed in Table 1.

In this paper, we use the IllustrisTNG simulation to investigate the  $DM_{\text{host}}$  of FRBs. The IllustrisTNG project is a successor of the Illustris project. Using the moving mesh code AREPO, they perform a cosmological magnetohydrodynamical simulation (Pillepich et al. 2018a). Multiple physical processes that derive galaxy formation are implemented in AREPO. Several simulations are performed in this project. Each simulation contains a large number of simulated galaxies, and detailed information on each one of these galaxies is provided.

This paper is organized as follows. In section 2, we introduce the IllustrisTNG simulation and give the method to derive  $DM_{\text{host}}$ . We will present the  $DM_{\text{host}}$  distributions for repeating FRBs like FRB 121102 in section 3, repeating FRBs like FRB 180916 in section 4 and non-repeating FRBs in section 5. In section 6, the effect of selection criteria of galaxies is discussed and the redshifts of simulated FRBs are derived based on our results. Finally, conclusions are given in section 7.

## 2. METHOD

The DM in the FRB rest frame can be derived through

$$DM = \int n_e dl, \quad (2)$$

where  $n_e$  is the electron number density and  $dl$  is the light path. If the electron distribution of a galaxy is known, the  $DM_{\text{host}}$  can be derived through Equation 2. However, the electron distribution of a galaxy can hardly be obtained from observations. Therefore, the IllustrisTNG simulation is used to derive the electron distribution.

The IllustrisTNG project is a successor of the Illustris project. It is a large-volume, cosmological and magnetohydrodynamical simulation. It consists of TNG50, TNG100, and TNG300, which mean that the lengths of the simulation boxes are about 50 Mpc, 100 Mpc, and 300 Mpc, respectively. The large simulation box can be used to study the large-scale structure of the Universe, while the small simulation box can provide a better resolution of galaxies, which is important when we are interested in the structure of galaxies. Therefore, the TNG50 simulation is the best choice to derive the distribution of  $DM_{\text{host}}$ . However, as the data of TNG50 has not been released, we choose the data of TNG100 to perform the analysis, which has been released (Nelson et al. 2018; Pillepich et al. 2018b; Naiman et al. 2018; Nelson et al. 2018; Marinacci et al. 2018; Springel et al. 2018). The TNG100 includes three runs with different numbers of particles, which are called TNG100-1, TNG100-2, and TNG100-3, respectively. Among these three runs, we choose the TNG100-1, which contains the most particles. The side length of this run is 110.7 Mpc and it contains 6,028,568,000 dark matter particles. A good particle resolution can be achieved in this run. The initial conditions of this run are consistent with the Planck 2015 results (Planck Collaboration et al. 2016). The same cosmological parameters are also used in this paper.

Employing the friends-of-friends (FoF) algorithm, the dark matter particles in the TNG simulation are divided into different FoF halos (groups). In each halo, the particles are separated into subhalos using the subfind algorithm and the subhalos correspond to galaxies. For each subhalo, the TNG

project provides detailed information, such as the stellar mass, SFR, gas metallicity, half mass radius, etc. This information can help us to select similar galaxies to the observed FRB host galaxies. Repeating FRBs and non-repeating FRBs may occur in different types of galaxies. According to mass and SFR, we select galaxies that are similar to the host galaxies of localized FRBs. The details will be shown in the following sections. The data of each subhalo is divided into several parts, including gas, dark matter, tracers, black holes, stars, and wind particles. We download the gas part of the selected subhalos. The TNG simulation uses Voronoi tessellation to construct the geometry of finite volume. The information of each Voronoi cell is given by the TNG simulation. According to the simulation, the electron number density of each cell can be derived.

The electron number density of the non-star-forming cells can be obtained as follows. The TNG simulation provides the information needed to calculate the electron number density. According to the simulation, the electron number density  $n_e$  can be derived by

$$n_e = \eta_e X_H \frac{\rho}{m_H}. \quad (3)$$

where  $\eta_e$  is the electron abundance,  $\rho$  is the mass density,  $m_H$  is the mass of hydrogen atom, and  $X_H$  is hydrogen abundance of each Voronoi cell. But for star-forming cells, the electron abundance  $\eta_e$  given by the TNG simulation is not reliable. In this case, we consider the subgrid model proposed by [Springel & Hernquist \(2003\)](#), which is also adopted by the TNG simulation. According to this model, the multi-phase interstellar medium is comprised of a cold cloud and hot gas. In our calculation, we assume that the cold cloud is entirely neutral and the hot gas is totally ionized. This assumption has been used in many previous works ([Pakmor et al. 2018](#); [Stevens et al. 2019](#)). The fraction of hot gas is calculated according to [Springel & Hernquist \(2003\)](#). The method has been discussed in [Springel & Hernquist \(2003\)](#) and the appendix of [Stevens et al. \(2019\)](#). Assuming that the hot gas is totally ionized, we derive the electron number density of star-forming cells. The electron distribution in one Voronoi cell is assumed to be uniform, so each region in one Voronoi cell shares the same electron number density. Therefore, the  $DM_{\text{host}}$  in the local frame can be written as

$$DM_{\text{host}} = \int n_e dl = \sum_i^N n_{e,i} \Delta l_i, \quad (4)$$

where  $i$  refers to the  $i$ th Voronoi cell,  $l_i$  is the length of the light travel in the  $i$ th cell, and  $N$  is the total number of the cells which the light travels through.

Because the TNG simulation does not provide a clear boundary of subhalo, we use the following method to set the boundary of integration. When we try to get the  $DM_{\text{host}}$  of a subhalo, all the cells in parent halo are selected to analyze. The light of an FRB is emitted from a cell of this subhalo and propagates in a random direction. If the light travels into a cell which does not belong to this subhalo, we stop the integration.

The location of FRB in the host galaxy is important. Repeating FRBs and non-repeating FRBs may have different locations in their host galaxies. The positions of FRBs may strongly depend on the progenitor models. We will discuss the positions in detail later.

The TNG simulation contains 100 snapshots at different redshifts for each run. Among these snapshots, 20 snapshots are full and the remaining 80 are mini. Only the full snapshots are considered in our calculation. The current observations show that more than 90% of FRBs have the pseudo

redshifts  $z < 1.5$ . Thus, only the snapshots with  $z < 1.5$  are selected to analyze. According to these criteria, we select the snapshots with redshifts  $z = 0.1, 0.2, 0.3, 0.4, 0.5, 0.7, 1.0$  and  $1.5$ . In each snapshot, 1000 subhalos are selected to derive  $DM_{\text{host}}$  for repeating FRBs like FRB 121102. But for non-repeating FRBs and repeating FRBs like FRB 180916, in order to save calculation time, 200 subhalos are selected. For each subhalo, we simulate the positions of 500 FRBs and each 10 random propagating directions are simulated for each FRB. The details are discussed in the following sections. The evolution of  $DM_{\text{host}}$  as a function of redshift is also studied. In our calculation, we use PyTorch and GPU to accelerate the calculation.

### 3. REPEATING FRBS LIKE FRB 121102

So far, twenty repeating FRBs have been published (Spitler et al. 2014, 2016; CHIME/FRB Collaboration et al. 2019b,c; Fonseca et al. 2020). FRB 121102 is the first observed repeating FRBs. It has been localized to a dwarf galaxy with stellar mass about  $4 - 7 \times 10^7 M_{\odot}$  and SFR about  $0.4 M_{\odot} \text{ yr}^{-1}$  (Tendulkar et al. 2017). Recently, repeating FRB 180916 was localized to a spiral galaxy (Marcote et al. 2020), which is dramatically different from FRB 121102. The stellar mass of this galaxy is about  $10^{10} M_{\odot}$  and the SFR of the region around FRB 180916 is greater than  $0.016 M_{\odot} \text{ yr}^{-1}$ . The properties of these two galaxies are dramatically different, so we will discuss them separately. In this section, we choose the host galaxy of FRB 121102 as a typical host galaxy. The case of FRB 180916 will be discussed in the next section. We select 1000 subhalos with the stellar mass  $1 - 50 \times 10^7 M_{\odot}$  and the SFR  $0.1 - 0.7 M_{\odot} \text{ yr}^{-1}$ . The total masses of the selected galaxies are also collected, which include the mass contributed by gas, stars, dark matter, and black holes. Among these components, dark matter is the main contributor. The median and the  $1\sigma$  error of the total mass are given in Table 2.

It is difficult to determine the location of FRB in the galaxy. Some models suggest that repeating FRBs originate from the newborn neutron stars (Lyubarsky 2014; Metzger et al. 2017). Recently, a faint FRB 200428 has been discovered associated with a Galactic magnetar SGR 1935+2154 (The CHIME/FRB Collaboration et al. 2020; Bochenek et al. 2020). It supports the magnetar origin of FRBs. Newborn neutron stars are mainly produced by the core-collapse supernovae and the formation rate may trace the SFR. Therefore, we assume that the probability of FRBs occurring in a cell is proportional to the SFR. For simplicity, we also assume that FRBs only occur at the centers of cells. According to this scenario, 500 positions of FRBs are simulated in each selected galaxy. For each simulated FRB, ten propagation directions are randomly selected in its rest frame. As a result, about  $5 \times 10^6$   $DM_{\text{host}}$  are derived at each redshift. Considering the cosmological evolution, the observed  $DM_{\text{host}}$  can be computed. The  $DM_{\text{host}}$  distribution at  $z = 0.2$  is shown in Figure 1 as an example. As for the  $DM_{\text{host}}$  distributions at other redshifts, they have a similar shape but different parameters. We only list the medians and the  $1\sigma$  errors of these distributions in Table 2. Besides, the evolution of  $DM_{\text{host}}$  with redshifts is important. We show the median and the  $1\sigma$  error at each redshift in the left panel of Figure 2 as the blue line.

From Figure 1, it is obvious that the distribution of  $DM_{\text{host}}$  has a long tail. Due to this reason, the median of  $DM_{\text{host}}$  is more representative than the mean value. Tendulkar et al. (2017) obtained the  $DM_{\text{host}}$  of FRB 121102 between 55 and 225  $\text{pc cm}^{-3}$  at redshift  $z = 0.193$ . We show this  $DM_{\text{host}}$  with the blue shaded region in Figure 1. In our simulation, the  $DM_{\text{host}}$  at  $z = 0.2$  is  $42.81_{-26.09}^{+50.73} \text{ pc cm}^{-3}$ , which is consistent with the observation at  $1\sigma$  confidence level. It must be noted that the value of  $DM_{\text{source}}$  of FRB 121102 may be large. From observations, the rotation measure (RM) of

FRB 121102 is very large, which is about  $10^5$  rad m $^{-2}$  (Michilli et al. 2018). This large RM originates from the local environment, which suggests a large  $DM_{\text{source}}$ . The  $DM_{\text{host}}$  given by Tendulkar et al. (2017) includes the contribution from the environment around the source. Thus, the DM contributed by the host galaxy must be smaller. Meanwhile, it has been shown that the host galaxy of FRB 121102 is atypical among nearby FRBs (Li et al. 2019a). The possible  $DM_{\text{host}}$  of repeating FRB 180814 is given in their work, which is  $DM_{\text{host}} < 80$  pc cm $^{-3}$ . This is also consistent with our results. The distribution of  $DM_{\text{host}}$  has a long tail, which indicates some light paths pass through the whole galaxy. The values of DMs along these directions are very large. We use the log-normal function to fit the distribution of  $DM_{\text{host}}$ ,

$$P(x; \mu, \sigma) = \frac{1}{x\sigma\sqrt{2\pi}} \exp\left(-\frac{(\ln x - \mu)^2}{2\sigma^2}\right), \quad (5)$$

where  $\mu$  and  $\sigma$  are free parameters. The mean and variance of this distribution are  $e^\mu$  and  $e^{(2\mu+\sigma^2)}[e^{\sigma^2} - 1]$ , respectively. In Figure 1, the red line is the best-fitting result and the fitting parameters are listed in Table 3.

We also find that  $DM_{\text{host}}$  increase as redshifts increase. The evolution of the median of  $DM_{\text{host}}$  can be fitted by

$$DM_{\text{host}}(z) = A(1+z)^\alpha. \quad (6)$$

The best fitting parameters are  $A = 34.72_{-14.47}^{+17.77}$  pc cm $^{-3}$ , and  $\alpha = 1.08_{-0.70}^{+0.87}$ . The fitting result is shown as the red dashed line in the left panel of Figure 2. In order to investigate this evolution, we show the comoving electron number density at different redshifts in Figure 3. At each redshift, we collect the electron number density of each cell for the selected subhalos. The red solid line and the red shaded region are the median and  $1\sigma$  uncertainty of the electron number density, respectively. The comoving electron number density decreases slowly with the increases of redshift. This evolution is so small that we can safely neglect it. Considering the cosmological evolution, the local electron number density at high redshift is much higher. Besides, we also should consider the factor  $(1+z)$  when the local  $DM_{\text{host}}$  is converted to the observed one. These effects cause the redshift evolution of  $DM_{\text{host}}$ . We also count the number of gas cells in each subhalo and show the result in Figure 3. The blue dashed line is the median and the blue shaded region is the  $1\sigma$  error of the number. The number of cells remains constant for all redshifts. Thus, it has no contribution to the  $DM_{\text{host}}$  evolution.

The mass resolution of IllustrisTNG100 is  $7.5 \times 10^6 M_\odot$  in dark matter particles and  $1.4 \times 10^6 M_\odot$  in gas particles<sup>1</sup>. In our work, it is important to test the completeness of the halo catalogue we used at the low-mass end. To do this, we compare the measured halo mass function from the simulation with the analytical fitting formula proposed by Tinker (Tinker et al. 2008). As the Tinker mass function only works for a dark matter only simulation, in this test we use the IllustrisTNG100 dark matter only run instead of the full baryonic ones. Figure 4 compares the halo mass function of the IllustrisTNG100 simulation (black solid line) with the Tinker’s fitting formula (blue solid line). The results agree very well at the low mass end, which indicates that the resolved halos in the IllustrisTNG100 are complete down to  $10^9 M_\odot$ .

#### 4. REPEATING FRBS LIKE FRB 180916

<sup>1</sup> <https://www.tng-project.org/about/>

The host galaxy of FRB 180916 is dramatically different from FRB 121102. It indicates that repeating FRBs can occur in various galaxies. In this section, we investigate the distribution of  $DM_{\text{host}}$  for the host galaxies like FRB 180916. This host galaxy is a spiral galaxy with stellar mass about  $10^{10} M_{\odot}$  (Marcote et al. 2020). This repeating FRB was born in a star-forming region. The total SFR of this galaxy is not given in their work, but they give the SFR of a small region, which is greater than  $0.016 M_{\odot} \text{ yr}^{-1}$ . In our analysis, the subhalos with stellar mass about  $(0.1 - 10) \times 10^{10} M_{\odot}$  are selected. The total SFR of the host galaxy is not clear, therefore, we adopt a wide range of SFR  $0.01 - 10 M_{\odot} \text{ yr}^{-1}$ . In order to save the calculation time, only 200 subhalos are selected for each redshift. Again, 500 FRB positions are simulated and 10 propagating directions are randomly selected for each FRB. FRB 180916 is born in a star-forming region. Therefore, we assume that the probability of FRBs borning in a cell traces the SFR of this cell. This assumption agrees with the case of repeating FRBs like FRB 121102. The distribution of  $DM_{\text{host}}$  at  $z = 0.1$  is shown in Figure 5 and the medians at different redshifts are shown in the middle panel of Figure 2 as the blue solid line. We also list the median and  $1\sigma$  range at different redshifts in Table 2. The shapes of distributions at other redshifts are similar to the distribution at  $z = 0.1$ . The log-normal function (Equation 5) is used to fit the distribution of  $DM_{\text{host}}$  and the best-fitting parameters are listed in Table 3.

In this case, the  $DM_{\text{host}}$  at  $z = 0.1$  is about  $110 \text{ pc cm}^{-3}$  and the  $1\sigma$  region is about  $30 - 250 \text{ pc cm}^{-3}$ . Marcote et al. (2020) estimate the  $DM_{\text{host}}$  less than  $70 \text{ pc cm}^{-3}$  for FRB 180916, which is consistent with our results at  $1\sigma$  level. In Figure 5, the blue shaded region denotes the  $DM_{\text{host}}$  of FRB 180916. Due to face-on view (Marcote et al. 2020), the  $DM_{\text{host}}$  of FRB 180916 is very small. Besides, we find that the  $DM_{\text{host}}$  is larger than the results of host galaxies like FRB 121102. It is caused by the larger subhalos. The subhalos with larger stellar mass are selected in this case. They have more cells and the light travel paths in host galaxies are much longer. The similar evolution of  $DM_{\text{host}}$  with redshifts is also found. We use Equation (6) to fit the evolution of  $DM_{\text{host}}$ . The red dashed line in the middle panel of Figure 2 is the best fitting with  $A = 96.22_{-42.26}^{+50.10} \text{ pc cm}^{-3}$ , and  $\alpha = 0.83_{-0.58}^{+0.87}$ . This evolution is also caused by the cosmological effect. Similar to the previous case, the galaxies with high redshifts are much denser and the electron number densities at high redshifts are much higher. Besides, the evolution factor  $(1 + z)$  needs to be considered when convert the local  $DM_{\text{host}}$  to the observed one. These cosmological effects cause the evolution of  $DM_{\text{host}}$ .

## 5. NON-REPEATING FRBS

Recently, seven apparently non-repeating FRBs have been localized (Bannister et al. 2019; Ravi et al. 2019; Prochaska et al. 2019; Macquart et al. 2020). The host galaxies of these FRBs are similar. The stellar mass is in the range  $10^9 - 10^{11} M_{\odot}$  and the SFR is in the range  $0 - 2 M_{\odot} \text{ yr}^{-1}$ . Based on these observations, we select 200 subhalos with stellar mass between  $10^9 M_{\odot}$  and  $2 \times 10^{11} M_{\odot}$ , and SFR in the range  $0 - 2 M_{\odot} \text{ yr}^{-1}$ . Similar to repeating FRBs, the locations of non-repeating FRBs are important and difficult to determine. Their progenitor model is different from the repeating FRBs. There are many works suggesting that the non-repeating FRBs originate from the merger of compact binaries (i.e., Totani 2013; Wang et al. 2016). According to these models, the positions of non-repeating FRBs should follow the mergers of compact binaries. From observations, the positions of these FRBs are far from the centers of host galaxies (Bannister et al. 2019; Ravi et al. 2019; Prochaska et al. 2019; Macquart et al. 2020), which also supports the conjecture that they are produced by the binary neutron star mergers. We adopt the results of Wang et al. (2020). Assuming that FRBs are produced by the mergers of binary neutron stars, they calculated the locations of FRBs in different

types of galaxies through the population synthesis method (Wang et al. 2020). Because of the long merger time of binary neutron stars and the large kick velocity, the merger locations are far from the galaxy centers. We adopt their results for massive spiral galaxies with  $10^{11}M_{\odot}$  case. According to their results, we simulate 500 positions of FRBs in each galaxy. In the rest frame of each FRB, 10 random propagating directions are simulated.

For non-repeating FRBs, we show the distributions of  $DM_{\text{host}}$  in Figure 6. The distributions at the redshifts which close to the observed FRBs are shown. The median and  $1\sigma$  error at all redshifts are listed in Table 2. The long tails are shown in these distributions, which is similar to repeating FRBs. The log-normal function (Equation 5) is used to fit these distributions and the fitting results are shown as the red lines in Figure 6. We also list the best-fitting parameters in Table 3. In this case, the stellar mass is similar to the case of repeating FRBs like FRB 180916, but the value of  $DM_{\text{host}}$  is different, which is caused by the different locations. For non-repeating FRBs, we simulate the positions according to Wang et al. (2020). Thus, the simulated FRBs are located at the edges of the galaxies and the  $DM_{\text{host}}$  is small. Based on the observations of host galaxies, some  $DM_{\text{host}}$  have been given in previous works (Ravi et al. 2019; Bannister et al. 2019; Chittidi et al. 2020). We show these values in Figure 6 with the blue shaded regions. Assuming a narrow luminosity distribution, Yang et al. (2017) gave the relation between  $DM_{\text{host}}$ , observed flux and luminosity. They found  $DM_{\text{host}}$  to be  $267.00_{-110.68}^{+172.53}$  pc cm $^{-3}$ , which is different from our results. This may be caused by their strong assumption on the luminosity distribution. They assumed that the luminosity function is very narrow. However, Luo et al. (2018) found that the luminosity function spans a large range. This wide range of luminosity function has also been found by Agarwal et al. (2019). Li et al. (2019a) also give similar results for some non-repeating FRBs. In their calculation, some possible  $DM_{\text{host}}$  for the selected FRBs are given, which are about 10 – 120 pc cm $^{-3}$ . We also show the relation between  $DM_{\text{host}}$  and redshift in the right panel of Figure 2 with the blue solid line. In this case,  $DM_{\text{host}}$  increases as redshift increases. We use equation 6 to fit this evolution. The fitting result is shown in the right panel of Figure 2 with the red dashed line and the best-fitting parameters are  $A = 32.97_{-17.65}^{+23.23}$  pc cm $^{-3}$  and  $\alpha = 0.84_{-0.60}^{+0.93}$ . Like the previous cases, this evolution is also caused by the cosmological effects.

## 6. DISCUSSIONS

### 6.1. The selection of host galaxy

In our calculation, we select host galaxies according to the stellar mass and the SFR. Based on the observation of FRB 121102 (Tendulkar et al. 2017), the galaxies with stellar mass  $1 - 50 \times 10^7 M_{\odot}$  and SFR  $0.1 - 0.7 M_{\odot} \text{ yr}^{-1}$  are selected. In order to test the dependence of our results on the properties of galaxies, we select galaxies with a narrow range of stellar mass and SFR.

In order to compare with the observation of FRB 121102, we only select the subhalos with  $z = 0.2$  to analyze. The host galaxy of FRB 121102 is a dwarf galaxy with the stellar mass  $4 - 7 \times 10^7 M_{\odot}$  and the SFR about  $0.4 M_{\odot} \text{ yr}^{-1}$ . According to this observation, we limit the stellar mass in the range  $4 - 7 \times 10^7 M_{\odot}$  and the SFR in the range  $0.1 - 0.6 M_{\odot} \text{ yr}^{-1}$ . This range is narrower than we used above. In order to save the calculation time, 200 subhalos are selected. 500 positions of FRBs are simulated and 10 propagating directions are randomly selected. The result is shown as the blue histogram in the top left panel of Figure 7. For comparison, the red histogram for the wide range case (Figure 1) is also shown in the top right panel. These two histograms are compared in the bottom panel. It's



clear that these two histograms are consistent with each other. Therefore, if the ranges of the stellar mass and the SFR are compatible with observations, the result is reliable.

### 6.2. Recover the Distribution of Redshifts

An important application of our results is to derive the redshifts of non-localized FRBs. If the value of  $DM_{\text{host}}$  is known, the redshifts of FRBs can be determined according to the relation between  $DM_{\text{IGM}}$  and  $z$ . For a large sample of FRBs without measured redshifts, the distribution of redshifts for these FRBs can be recovered. In this section, we use our results to infer the pseudo redshifts of simulated FRBs and recover the distribution of redshifts.

Assuming the formation rate of FRBs traces the cosmic SFR (Madau & Dickinson 2014), we generate a mock FRB sample, which contains 500 FRBs with redshifts. Using the relation (Ioka 2003; Deng & Zhang 2014)

$$DM_{\text{IGM}}(z) = \frac{3cH_0\Omega_b}{8\pi Gm_p} f_{\text{IGM}} \int_0^z \frac{H_0 f_e(z')(1+z')}{H(z')} dz', \quad (7)$$

we can derive  $DM_{\text{IGM}}$  of these simulated FRBs. In this equation,  $f_{\text{IGM}} \simeq 0.83$  is the fraction of baryon mass in the IGM and  $f_e(z') \simeq 7/8$  is the number ratio between the free electrons and baryons in the IGM. We ignore the fluctuation of  $DM_{\text{IGM}}$ , which is complex and difficult to evaluate. As for  $DM_{\text{host}}$ , we use the distribution of  $DM_{\text{host}}$  for repeating FRBs like FRB 121102 as an example. In our results, only the distributions of  $DM_{\text{host}}$  at discrete redshifts have been obtained. For any given redshift  $z_1 < z < z_2$ , we calculate  $DM_{\text{host}}$  at  $z$  using the interpolation method

$$DM_{\text{host}}(z) = \frac{z_2 - z}{z_2 - z_1} DM_{\text{host}}(z_1) + \frac{z - z_1}{z_2 - z_1} DM_{\text{host}}(z_2), \quad (8)$$

where  $DM_{\text{host}}(z_1)$  and  $DM_{\text{host}}(z_2)$  are randomly selected from the samples which satisfies the distributions of  $DM_{\text{host}}$  at  $z_1$  and  $z_2$ . The Monte Carlo simulation is adopted to simulate  $DM_{\text{host}}$  of these simulated FRBs. Using this method, we simulate the  $DM_{\text{ex}} = DM_{\text{host}} + DM_{\text{IGM}}$  of this mock sample.

The probability that an FRB with  $DM_{\text{ex}}$  located at redshift  $z_1 < z < z_2$  is derived through the linear interpolation method, which is

$$P(DM_{\text{ex}}, z) = \frac{z_2 - z}{z_2 - z_1} P_{z_1}(DM_{\text{host}}) + \frac{z - z_1}{z_2 - z_1} P_{z_2}(DM_{\text{host}}), \quad (9)$$

where  $DM_{\text{host}} = DM_{\text{ex}} - DM_{\text{IGM}}$ ,  $P_{z_1}$  and  $P_{z_2}$  are the probability density functions of  $DM_{\text{host}}$  at redshifts  $z_1$  and  $z_2$ , respectively. The fluctuation of  $DM_{\text{IGM}}$  is ignored, so it can be derived from Equation 7.

We use the maximum likelihood method to derive the best-fit redshifts and show the results in Figure 8. The blue histogram is the distribution of the simulated redshifts and the red histogram is the derived redshifts. These two distributions are similar to each other. Moreover, there are small differences between the two distributions at both low redshifts and high redshifts. The reason is that the maximum likelihood method yields unreasonable results for those FRBs with high or extremely small DMs. Thus, we may lose some information at low and high redshifts.

## 7. CONCLUSIONS

In this paper, we use the IllustrisTNG simulation to derive the distributions of DMs contributed by the host galaxies of FRBs. Based on the observations of localized FRBs, we select galaxies to calculate the host galaxy DMs of FRBs. For repeating FRBs like FRB 121102, we select the galaxies with stellar mass in the range  $1 - 50 \times 10^7 M_\odot$  and SFR in the range  $0.1 - 0.7 M_\odot \text{ yr}^{-1}$ . Assuming the formation rate of repeating FRBs in a given cell is proportional to the SFR of this cell, 500 positions of FRBs are simulated in each galaxy. For each FRB, ten random propagating directions are selected. We derive the distributions of  $\text{DM}_{\text{host}}$  at different redshifts and show the result at  $z = 0.2$  in Figure 1. The observed  $\text{DM}_{\text{host}}$  of FRB 121102 is also shown in Figure 1 with the blue shaded region. In addition, the evolution of the median with redshifts is shown in Figure 2. We find that the value of  $\text{DM}_{\text{host}}$  increases as redshift increases. We also select subhalos according to the host galaxy of repeating FRB 180916. The host galaxy of this FRB is dramatically different from FRB 121102. Therefore, we analyze it separately. The result is shown in Figure 5 and we compare our results with the observation. In this case, the  $\text{DM}_{\text{host}}$  also increases as redshift increases, which is caused by the cosmological evolution.

For non-repeating FRBs, we select the galaxies with masses in the range  $10^9 - 2 \times 10^{11} M_\odot$  and SFRs in the range  $0 - 2 M_\odot \text{ yr}^{-1}$ , which are similar to the observed non-repeating FRB host galaxies. Assuming that the burst sites are the locations of binary neutron star mergers, we generate 500 FRBs positions in each galaxy. The distributions of  $\text{DM}_{\text{host}}$  are shown in Figure 6 and listed in Table 2. The value of  $\text{DM}_{\text{host}}$  increases as redshift increases, which is caused by the cosmological evolution.

The effect of the selection criteria for galaxies is also discussed. We use a narrow range of the stellar mass and the SFR to investigate the distribution of  $\text{DM}_{\text{host}}$ . The distribution in this case is consistent with the results of the wide-parameters case. Thus, if the ranges of the stellar mass and the SFR are compatible with the observation, the width of parameter range would have little effect on the results. We also use our results to infer the pseudo redshifts of simulated FRBs and show that we can recover the distribution of simulated redshifts.

We thank the anonymous referee for constructive and helpful comments. This work is supported by the National Natural Science Foundation of China (grant U1831207). Hai Yu is supported by Initiative Postdocs Supporting Program (No. BX20190206).

## REFERENCES

- Agarwal, D., Lorimer, D. R., Fialkov, A., et al. 2019, *MNRAS*, 490, 1, doi: [10.1093/mnras/stz2574](https://doi.org/10.1093/mnras/stz2574)
- Bannister, K. W., Deller, A. T., Phillips, C., et al. 2019, *Science*, 365, 565, doi: [10.1126/science.aaw5903](https://doi.org/10.1126/science.aaw5903)
- Bochenek, C. D., Ravi, V., Belov, K. V., et al. 2020, arXiv e-prints, arXiv:2005.10828. <https://arxiv.org/abs/2005.10828>
- Caleb, M., Flynn, C., & Stappers, B. W. 2019, *MNRAS*, 485, 2281, doi: [10.1093/mnras/stz571](https://doi.org/10.1093/mnras/stz571)
- Chatterjee, S., Law, C. J., Wharton, R. S., et al. 2017, *Nature*, 541, 58, doi: [10.1038/nature20797](https://doi.org/10.1038/nature20797)
- CHIME/FRB Collaboration, Amiri, M., Bandura, K., et al. 2019a, *Nature*, 566, 230, doi: [10.1038/s41586-018-0867-7](https://doi.org/10.1038/s41586-018-0867-7)
- . 2019b, *Nature*, 566, 235, doi: [10.1038/s41586-018-0864-x](https://doi.org/10.1038/s41586-018-0864-x)
- CHIME/FRB Collaboration, Andersen, B. C., Bandura, K., et al. 2019c, *ApJL*, 885, L24, doi: [10.3847/2041-8213/ab4a80](https://doi.org/10.3847/2041-8213/ab4a80)
- Chittidi, J. S., Simha, S., Mannings, A., et al. 2020, arXiv e-prints, arXiv:2005.13158. <https://arxiv.org/abs/2005.13158>
- Cordes, J. M., & Chatterjee, S. 2019, *ARA&A*, 57, 417, doi: [10.1146/annurev-astro-091918-104501](https://doi.org/10.1146/annurev-astro-091918-104501)

- Cordes, J. M., & Lazio, T. J. W. 2002, arXiv e-prints, astro.  
<https://arxiv.org/abs/astro-ph/0207156>
- Deng, W., & Zhang, B. 2014, *ApJL*, 783, L35,  
 doi: [10.1088/2041-8205/783/2/L35](https://doi.org/10.1088/2041-8205/783/2/L35)
- Dolag, K., Gaensler, B. M., Beck, A. M., & Beck, M. C. 2015, *MNRAS*, 451, 4277,  
 doi: [10.1093/mnras/stv1190](https://doi.org/10.1093/mnras/stv1190)
- Fialkov, A., & Loeb, A. 2016, *JCAP*, 2016, 004,  
 doi: [10.1088/1475-7516/2016/05/004](https://doi.org/10.1088/1475-7516/2016/05/004)
- Fonseca, E., Andersen, B. C., Bhardwaj, M., et al. 2020, arXiv e-prints, arXiv:2001.03595.  
<https://arxiv.org/abs/2001.03595>
- Gao, H., Li, Z., & Zhang, B. 2014, *ApJ*, 788, 189,  
 doi: [10.1088/0004-637X/788/2/189](https://doi.org/10.1088/0004-637X/788/2/189)
- Ioka, K. 2003, *ApJL*, 598, L79,  
 doi: [10.1086/380598](https://doi.org/10.1086/380598)
- Jaroszynski, M. 2019, *MNRAS*, 484, 1637,  
 doi: [10.1093/mnras/sty3529](https://doi.org/10.1093/mnras/sty3529)
- Li, Y., Zhang, B., Nagamine, K., & Shi, J. 2019a, *ApJL*, 884, L26, doi: [10.3847/2041-8213/ab3e41](https://doi.org/10.3847/2041-8213/ab3e41)
- Li, Z., Gao, H., Wei, J.-J., et al. 2019b, *ApJ*, 876, 146, doi: [10.3847/1538-4357/ab18fe](https://doi.org/10.3847/1538-4357/ab18fe)
- Li, Z.-X., Gao, H., Ding, X.-H., Wang, G.-J., & Zhang, B. 2018, *Nature Communications*, 9, 3833, doi: [10.1038/s41467-018-06303-0](https://doi.org/10.1038/s41467-018-06303-0)
- Lorimer, D. R., Bailes, M., McLaughlin, M. A., Narkevic, D. J., & Crawford, F. 2007, *Science*, 318, 777, doi: [10.1126/science.1147532](https://doi.org/10.1126/science.1147532)
- Luo, R., Lee, K., Lorimer, D. R., & Zhang, B. 2018, *MNRAS*, 481, 2320,  
 doi: [10.1093/mnras/sty2364](https://doi.org/10.1093/mnras/sty2364)
- Lyubarsky, Y. 2014, *MNRAS*, 442, L9,  
 doi: [10.1093/mnrasl/slu046](https://doi.org/10.1093/mnrasl/slu046)
- Macquart, J. P., Prochaska, J. X., McQuinn, M., et al. 2020, *Nature*, 581, 391,  
 doi: [10.1038/s41586-020-2300-2](https://doi.org/10.1038/s41586-020-2300-2)
- Madau, P., & Dickinson, M. 2014, *ARA&A*, 52, 415, doi: [10.1146/annurev-astro-081811-125615](https://doi.org/10.1146/annurev-astro-081811-125615)
- Marcote, B., Nimmo, K., Hessels, J. W. T., et al. 2020, *Nature*, 577, 190,  
 doi: [10.1038/s41586-019-1866-z](https://doi.org/10.1038/s41586-019-1866-z)
- Margalit, B., Berger, E., & Metzger, B. D. 2019, *ApJ*, 886, 110, doi: [10.3847/1538-4357/ab4c31](https://doi.org/10.3847/1538-4357/ab4c31)
- Marinacci, F., Vogelsberger, M., Pakmor, R., et al. 2018, *MNRAS*, 480, 5113,  
 doi: [10.1093/mnras/sty2206](https://doi.org/10.1093/mnras/sty2206)
- Metzger, B. D., Berger, E., & Margalit, B. 2017, *ApJ*, 841, 14, doi: [10.3847/1538-4357/aa633d](https://doi.org/10.3847/1538-4357/aa633d)
- Michilli, D., Seymour, A., Hessels, J. W. T., et al. 2018, *Nature*, 553, 182,  
 doi: [10.1038/nature25149](https://doi.org/10.1038/nature25149)
- Muñoz, J. B., Kovetz, E. D., Dai, L., & Kamionkowski, M. 2016, *PhRvL*, 117, 091301,  
 doi: [10.1103/PhysRevLett.117.091301](https://doi.org/10.1103/PhysRevLett.117.091301)
- Naiman, J. P., Pillepich, A., Springel, V., et al. 2018, *MNRAS*, 477, 1206,  
 doi: [10.1093/mnras/sty618](https://doi.org/10.1093/mnras/sty618)
- Nelson, D., et al. 2018.  
<https://arxiv.org/abs/1812.05609>
- Nelson, D., Pillepich, A., Springel, V., et al. 2018, *MNRAS*, 475, 624, doi: [10.1093/mnras/stx3040](https://doi.org/10.1093/mnras/stx3040)
- Pakmor, R., Guillet, T., Pfrommer, C., et al. 2018, *MNRAS*, 481, 4410, doi: [10.1093/mnras/sty2601](https://doi.org/10.1093/mnras/sty2601)
- Petroff, E., Hessels, J. W. T., & Lorimer, D. R. 2019, *A&A Rv*, 27, 4,  
 doi: [10.1007/s00159-019-0116-6](https://doi.org/10.1007/s00159-019-0116-6)
- Petroff, E., Barr, E. D., Jameson, A., et al. 2016, *PASA*, 33, e045, doi: [10.1017/pasa.2016.35](https://doi.org/10.1017/pasa.2016.35)
- Pillepich, A., Springel, V., Nelson, D., et al. 2018a, *MNRAS*, 473, 4077, doi: [10.1093/mnras/stx2656](https://doi.org/10.1093/mnras/stx2656)
- Pillepich, A., Nelson, D., Hernquist, L., et al. 2018b, *MNRAS*, 475, 648,  
 doi: [10.1093/mnras/stx3112](https://doi.org/10.1093/mnras/stx3112)
- Piro, A. L. 2016, *ApJL*, 824, L32,  
 doi: [10.3847/2041-8205/824/2/L32](https://doi.org/10.3847/2041-8205/824/2/L32)
- Planck Collaboration, Ade, P. A. R., Aghanim, N., et al. 2016, *A&A*, 594, A13,  
 doi: [10.1051/0004-6361/201525830](https://doi.org/10.1051/0004-6361/201525830)
- Platts, E., Weltman, A., Walters, A., et al. 2019, *PhR*, 821, 1, doi: [10.1016/j.physrep.2019.06.003](https://doi.org/10.1016/j.physrep.2019.06.003)
- Prochaska, J. X., & Zheng, Y. 2019, *MNRAS*, 485, 648, doi: [10.1093/mnras/stz261](https://doi.org/10.1093/mnras/stz261)
- Prochaska, J. X., Macquart, J.-P., McQuinn, M., et al. 2019, arXiv e-prints, arXiv:1909.11681.  
<https://arxiv.org/abs/1909.11681>
- Ravi, V., Catha, M., D'Addario, L., et al. 2019, *Nature*, 572, 352,  
 doi: [10.1038/s41586-019-1389-7](https://doi.org/10.1038/s41586-019-1389-7)
- Shannon, R. M., Macquart, J. P., Bannister, K. W., et al. 2018, *Nature*, 562, 386,  
 doi: [10.1038/s41586-018-0588-y](https://doi.org/10.1038/s41586-018-0588-y)
- Spitler, L. G., Cordes, J. M., Hessels, J. W. T., et al. 2014, *ApJ*, 790, 101,  
 doi: [10.1088/0004-637X/790/2/101](https://doi.org/10.1088/0004-637X/790/2/101)
- Spitler, L. G., Scholz, P., Hessels, J. W. T., et al. 2016, *Nature*, 531, 202,  
 doi: [10.1038/nature17168](https://doi.org/10.1038/nature17168)

- Springel, V., & Hernquist, L. 2003, MNRAS, 339, 289, doi: [10.1046/j.1365-8711.2003.06206.x](https://doi.org/10.1046/j.1365-8711.2003.06206.x)
- Springel, V., Pakmor, R., Pillepich, A., et al. 2018, MNRAS, 475, 676, doi: [10.1093/mnras/stx3304](https://doi.org/10.1093/mnras/stx3304)
- Stevens, A. R. H., Diemer, B., Lagos, C. d. P., et al. 2019, MNRAS, 483, 5334, doi: [10.1093/mnras/sty3451](https://doi.org/10.1093/mnras/sty3451)
- Tendulkar, S. P., Bassa, C. G., Cordes, J. M., et al. 2017, ApJL, 834, L7, doi: [10.3847/2041-8213/834/2/L7](https://doi.org/10.3847/2041-8213/834/2/L7)
- The CHIME/FRB Collaboration, :, Andersen, B. C., et al. 2020, arXiv e-prints, arXiv:2005.10324, <https://arxiv.org/abs/2005.10324>
- Thornton, D., Stappers, B., Bailes, M., et al. 2013, Science, 341, 53, doi: [10.1126/science.1236789](https://doi.org/10.1126/science.1236789)
- Tinker, J. L., Kravtsov, A. V., Klypin, A., et al. 2008, Astrophys. J., 688, 709, doi: [10.1086/591439](https://doi.org/10.1086/591439)
- Totani, T. 2013, PASJ, 65, L12, doi: [10.1093/pasj/65.5.L12](https://doi.org/10.1093/pasj/65.5.L12)
- Walters, A., Weltman, A., Gaensler, B. M., Ma, Y.-Z., & Witzemann, A. 2018, ApJ, 856, 65, doi: [10.3847/1538-4357/aaaf6b](https://doi.org/10.3847/1538-4357/aaaf6b)
- Wang, F. Y., Wang, Y. Y., Yang, Y.-P., et al. 2020, ApJ, 891, 72, doi: [10.3847/1538-4357/ab74d0](https://doi.org/10.3847/1538-4357/ab74d0)
- Wang, J.-S., Yang, Y.-P., Wu, X.-F., Dai, Z.-G., & Wang, F.-Y. 2016, ApJL, 822, L7, doi: [10.3847/2041-8205/822/1/L7](https://doi.org/10.3847/2041-8205/822/1/L7)
- Wang, Y. K., & Wang, F. Y. 2018, A&A, 614, A50, doi: [10.1051/0004-6361/201731160](https://doi.org/10.1051/0004-6361/201731160)
- Wei, J.-J., Gao, H., Wu, X.-F., & Mészáros, P. 2015, PhRvL, 115, 261101, doi: [10.1103/PhysRevLett.115.261101](https://doi.org/10.1103/PhysRevLett.115.261101)
- Wei, J.-J., Li, Z., Gao, H., & Wu, X.-F. 2019, JCAP, 2019, 039, doi: [10.1088/1475-7516/2019/09/039](https://doi.org/10.1088/1475-7516/2019/09/039)
- Wu, Q., Yu, H., & Wang, F. Y. 2020, ApJ, 895, 33, doi: [10.3847/1538-4357/ab88d2](https://doi.org/10.3847/1538-4357/ab88d2)
- Yang, Y.-P., Luo, R., Li, Z., & Zhang, B. 2017, ApJL, 839, L25, doi: [10.3847/2041-8213/aa6c2e](https://doi.org/10.3847/2041-8213/aa6c2e)
- Yang, Y.-P., & Zhang, B. 2017, ApJ, 847, 22, doi: [10.3847/1538-4357/aa8721](https://doi.org/10.3847/1538-4357/aa8721)
- Yao, J. M., Manchester, R. N., & Wang, N. 2017, ApJ, 835, 29, doi: [10.3847/1538-4357/835/1/29](https://doi.org/10.3847/1538-4357/835/1/29)
- Yu, H., & Wang, F. Y. 2017, A&A, 606, A3, doi: [10.1051/0004-6361/201731607](https://doi.org/10.1051/0004-6361/201731607)
- Yu, H., Xi, S.-Q., & Wang, F.-Y. 2018, ApJ, 860, 173, doi: [10.3847/1538-4357/aac2e3](https://doi.org/10.3847/1538-4357/aac2e3)
- Zhang, B. 2020, ApJL, 890, L24, doi: [10.3847/2041-8213/ab7244](https://doi.org/10.3847/2041-8213/ab7244)
- Zhou, B., Li, X., Wang, T., Fan, Y.-Z., & Wei, D.-M. 2014, PhRvD, 89, 107303, doi: [10.1103/PhysRevD.89.107303](https://doi.org/10.1103/PhysRevD.89.107303)

**Table 1.** The properties of the known host galaxies of FRBs.

	FRB name	redshift	stellar mass ( $M_{\odot}$ )	SFR ( $M_{\odot} \text{ yr}^{-1}$ )	$\text{DM}_{\text{host}}$ ( $\text{pc cm}^{-3}$ )
Repeating	FRB 121102	0.19	$4 - 7 \times 10^7$	0.4	55-225
	FRB 180916	0.03	$\sim 10^{10}$	0.016*	<70
Non-Repeating	FRB 190523	0.66	$10^{11.07}$	<1.3	<150
	FRB 180924	0.32	$2.2 \times 10^{10}$	<2	30-81
	FRB 181112	0.48	$2.6 \times 10^9$	0.6	-
	FRB 190102	0.29	$10^{9.5}$	1.5	-
	FRB 190608	0.12	$10^{10.4}$	1.2	$137 \pm 43$
	FRB 190611	0.38	-	-	-
	FRB 190711	0.52	-	-	-

\*This is the SFR of the region where FRB 180916 was born. It corresponds to a region of  $1.5 \text{ kpc}^2$ .

Redshifts	$\text{DM}_{\text{host}}$ ( $\text{pc cm}^{-3}$ ) (like FRB 121102)	total mass $\times 10^{10} M_{\odot}$ , repeating	$\text{DM}_{\text{host}}$ ( $\text{pc cm}^{-3}$ ) (like FRB 180916)	$\text{DM}_{\text{host}}$ ( $\text{pc cm}^{-3}$ ) (non-repeating)
0.1	$35.14^{+42.19}_{-21.46}$	$0.09^{+0.11}_{-0.03}$	$110.96^{+141.89}_{-76.27}$	$38.83^{+109.34}_{-29.16}$
0.2	$42.81^{+50.73}_{-26.09}$	$0.10^{+1.89}_{-0.04}$	$126.84^{+162.08}_{-82.01}$	$44.92^{+114.43}_{-34.16}$
0.3	$49.35^{+55.15}_{-29.62}$	$0.08^{+0.15}_{-0.03}$	$138.13^{+158.63}_{-89.57}$	$46.92^{+122.82}_{-35.55}$
0.4	$55.29^{+60.37}_{-32.94}$	$0.09^{+0.61}_{-0.04}$	$139.44^{+162.88}_{-85.78}$	$53.87^{+129.07}_{-42.34}$
0.5	$61.79^{+65.64}_{-36.46}$	$0.10^{+0.53}_{-0.05}$	$154.09^{+167.26}_{-93.85}$	$57.49^{+128.12}_{-44.87}$
0.7	$74.77^{+76.07}_{-43.35}$	$0.09^{+1.82}_{-0.03}$	$155.24^{+190.64}_{-94.75}$	$56.59^{+122.63}_{-43.12}$
1	$90.70^{+90.79}_{-50.87}$	$0.12^{+3.49}_{-0.06}$	$170.07^{+222.19}_{-101.80}$	$63.60^{+137.01}_{-48.59}$
1.5	$106.48^{+112.50}_{-59.62}$	$0.33^{+3.20}_{-0.26}$	$221.51^{+323.08}_{-138.54}$	$69.47^{+170.33}_{-53.15}$

**Table 2.** The median  $\text{DM}_{\text{host}}$  with  $1\sigma$  uncertainty at different redshifts for repeating and non-repeating FRBs. We also give the total masses (median and  $1\sigma$  uncertainty) of the selected galaxies for repeating FRBs like FRB 121102.

redshifts	Repeating Like FRB 121102		Repeating Like FRB 180916		Non-Repeating	
	$e^{\mu}$ ( $\text{pc cm}^{-3}$ )	$\sigma$	$e^{\mu}$ ( $\text{pc cm}^{-3}$ )	$\sigma$	$e^{\mu}$ ( $\text{pc cm}^{-3}$ )	$\sigma$
0.1	35.33	0.82	96.37	0.97	36.55	1.27
0.2	43.07	0.80	121.17	0.89	40.10	1.25
0.3	49.72	0.76	127.16	0.86	42.30	1.23
0.4	55.55	0.76	140.58	0.80	43.60	1.29
0.5	62.18	0.75	155.57	0.82	47.47	1.29
0.7	75.17	0.73	157.68	0.84	48.44	1.21
1.0	90.77	0.73	159.56	0.84	53.87	1.20
1.5	105.74	0.75	218.74	0.90	60.98	1.24

**Table 3.** The best-fitting parameters with log-normal function of  $\text{DM}_{\text{host}}$  for different cases.

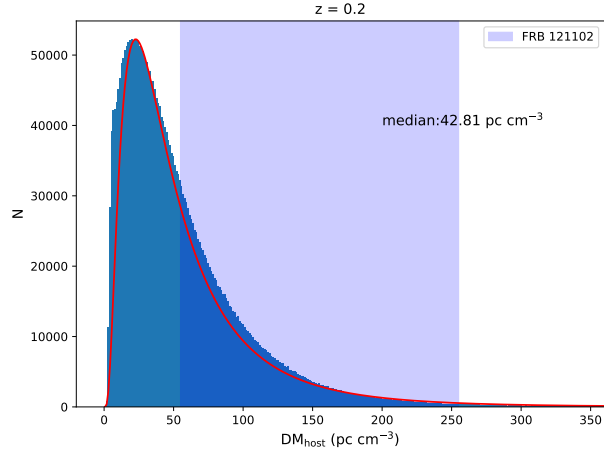


**Figure 1.** The distribution of  $DM_{\text{host}}$  at  $z = 0.2$  for repeating FRBs like FRB 121102. The red line is the best-fitting result using log-normal distribution. The best-fitting parameters are listed in Table 3. The blue shaded region is the  $DM_{\text{host}}$  for FRB 121102 inferred from the observation.

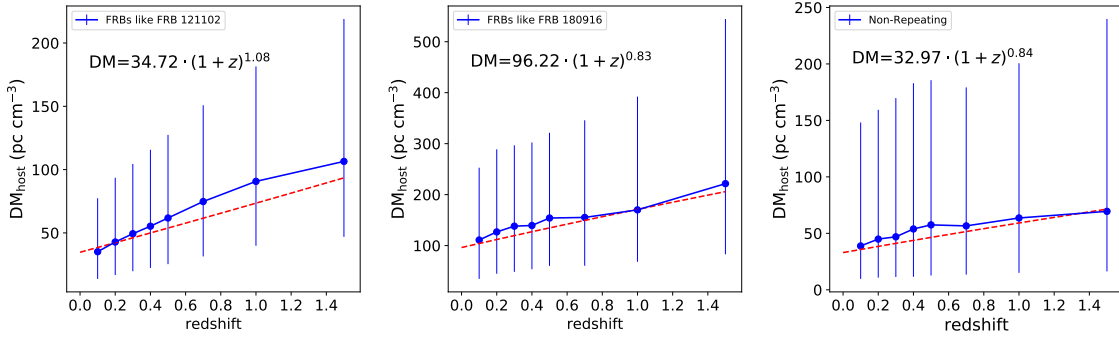


**Figure 2.** The median and  $1\sigma$  error of  $DM_{\text{host}}$  at different redshifts for three cases. The blue solid lines in the three panels are the evolutions of  $DM_{\text{host}}$  for repeating FRBs like FRB 121102, like FRB 180916 and non-repeating FRBs, respectively. The red dashed lines are the best-fitting results using equation (6) for three cases. The fitting results are shown in the figure.

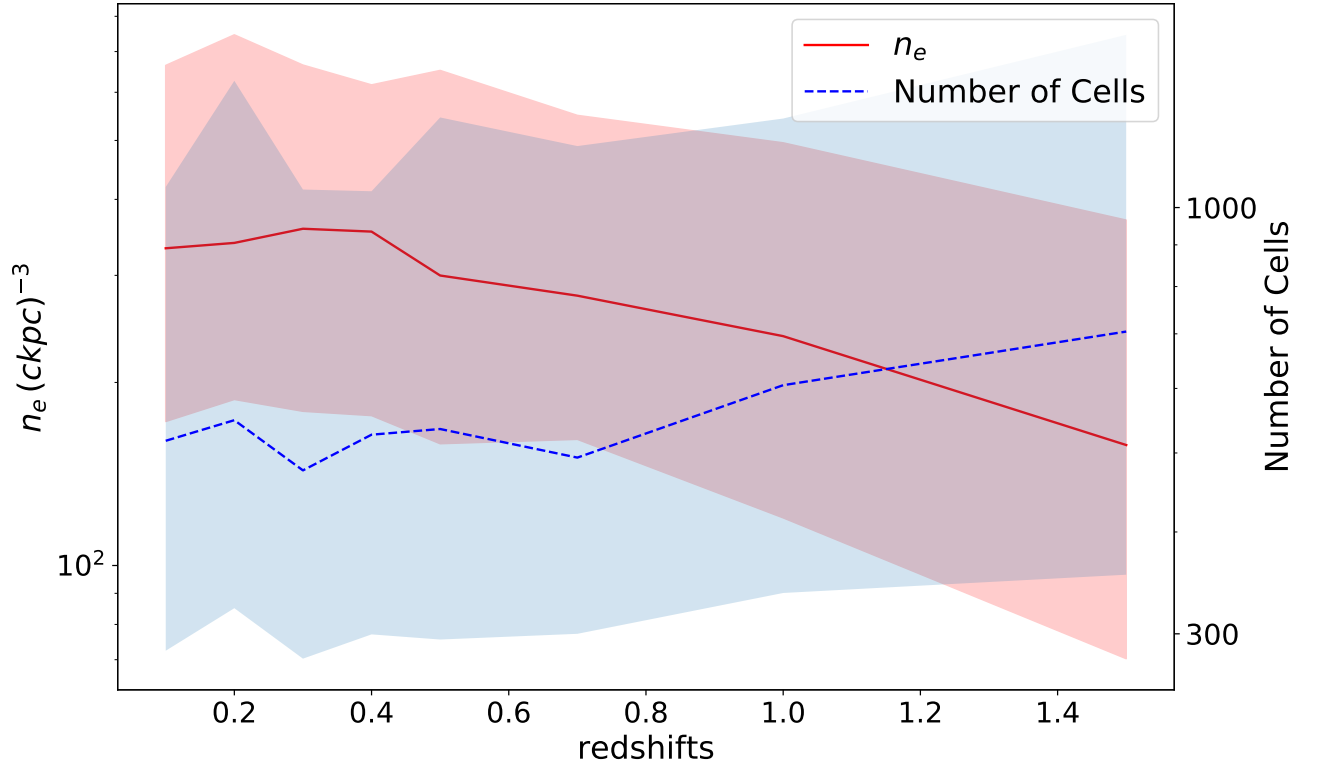


**Figure 3.** The comoving electron number density  $n_e$  and the number of cells in subhalos as a function of redshifts. These values are derived from the subhalos which are similar to the host galaxies of FRB 121102. The red solid line is median value of  $n_e$  with  $1\sigma$  error (red shaded region). The blue dashed line is the median with  $1\sigma$  error (blue shaded region) of the number of cells in subhalos.

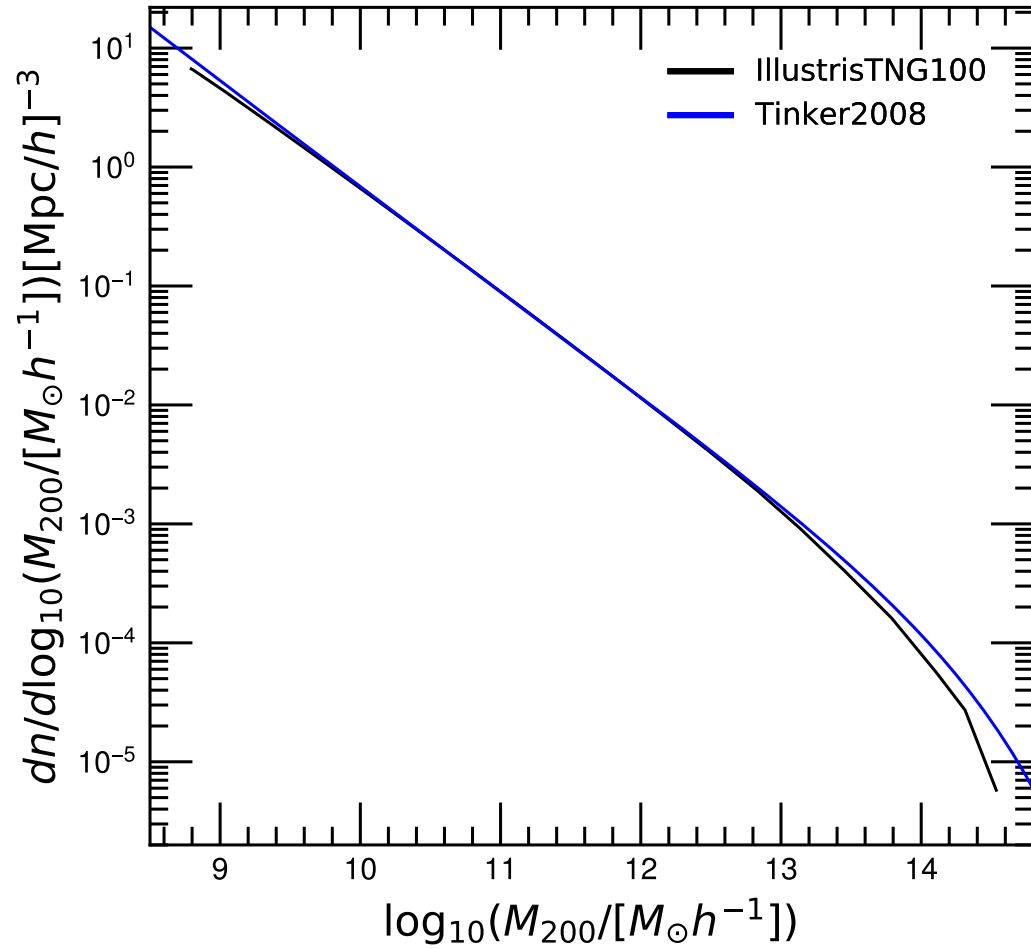


**Figure 4.** The halo mass function of the IllustrisTNG100 simulation versus the Tinker mass function. The two curves agree very well at the low-mass end, which indicates that the resolved halos in the IllustrisTNG100 is rather complete. The differences at the high-mass end are due to the limited box size of the IllustrisTNG100 simulation, which misses the most massive clusters in the universe.



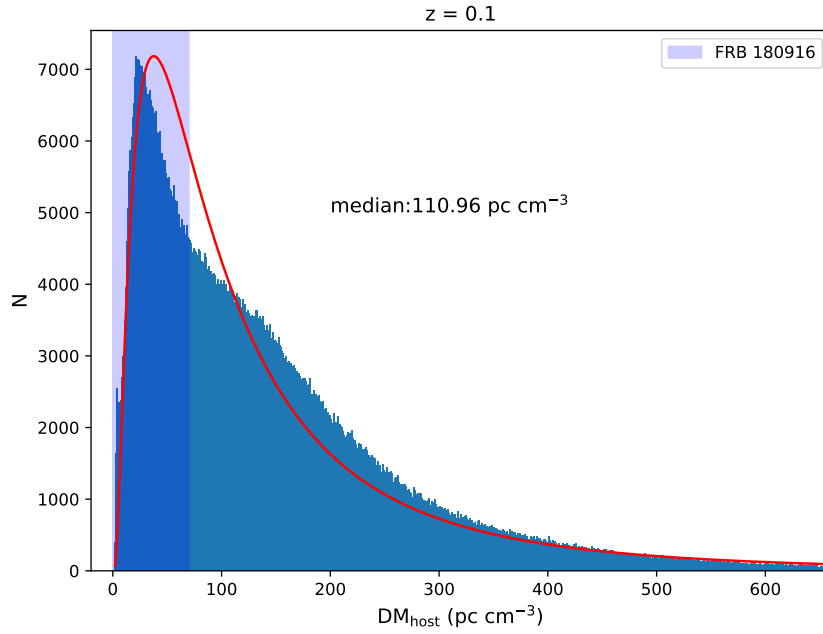


**Figure 5.** The distribution of  $DM_{\text{host}}$  at  $z = 0.1$  for repeating FRBs like FRB 180916. The red lines are the best-fitting results using log-normal distribution. The best-fitting parameters are listed in Table 3. The blue shaded region is the  $DM_{\text{host}}$  for FRB 180916 inferred from the observation.

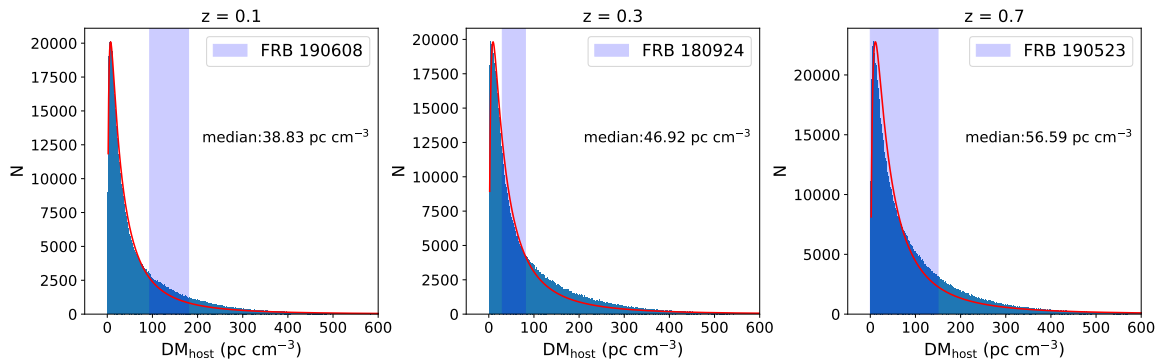


**Figure 6.** The distributions of  $DM_{\text{host}}$  for non-repeating FRBs at  $z = 0.1, 0.3,$  and  $0.7$ . The red lines are the best-fitting results using log-normal distribution and the best-fitting parameters are listed in table 3. The blue shaded regions are the  $DM_{\text{host}}$  inferred from observations.

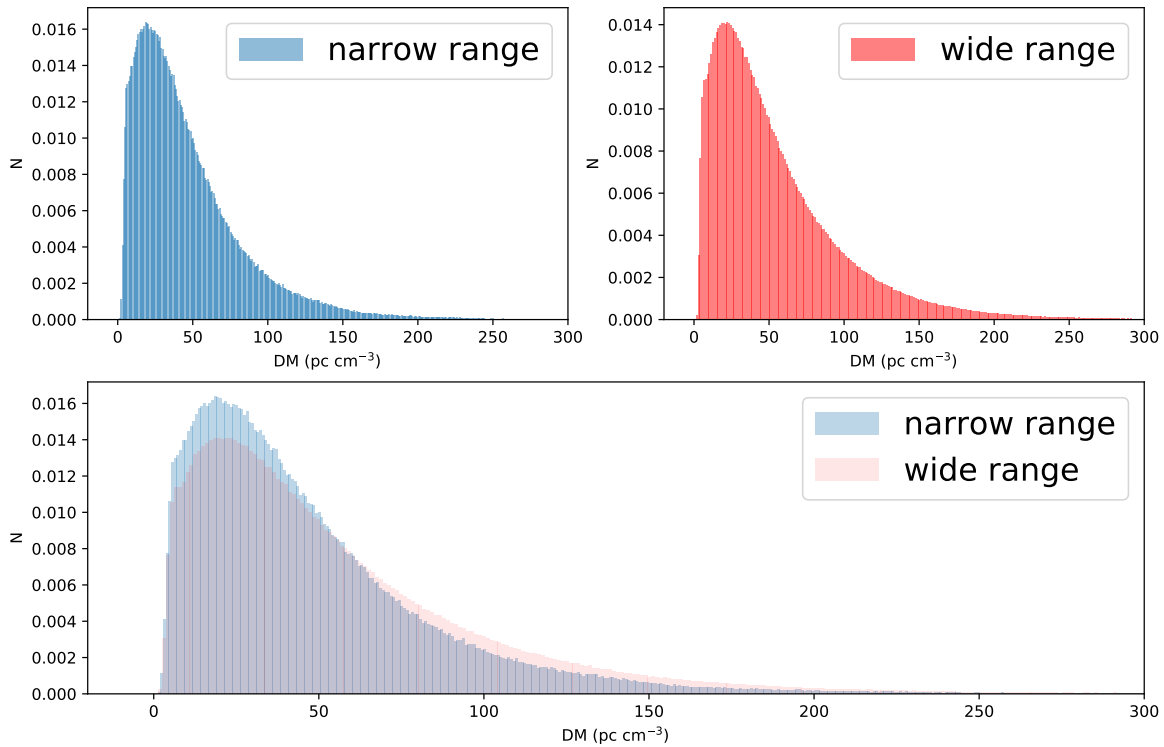


**Figure 7.** The distribution of  $DM_{\text{host}}$  for repeating FRBs at  $z = 0.2$  for different stellar masses and SFRs. The blue histogram in the top-left panel is derived from 200 galaxies with the stellar mass  $4 - 7 \times 10^7 M_{\odot}$  and SFR  $0.1 - 0.6 M_{\odot} \text{ yr}^{-1}$ . The red histogram in the top-right panel is the previous results shown in Figure 1. We also plot these two histograms in the bottom panel. These two histograms are consistent with each other.

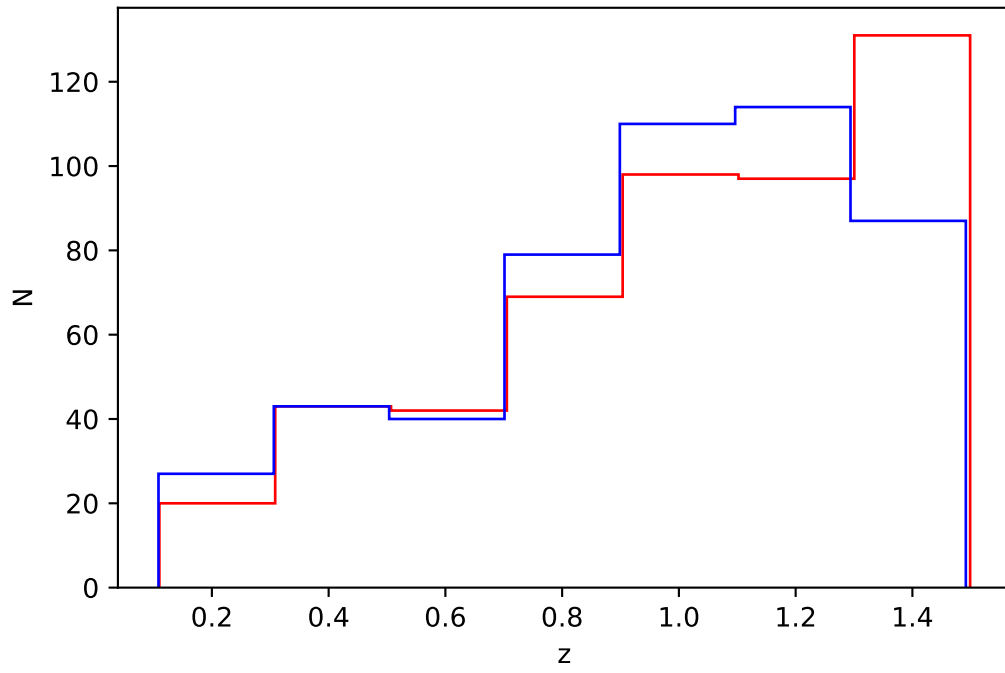


**Figure 8.** The histograms of simulated redshifts (blue) and derived redshifts (red) of FRBs. The two distributions are consistent with each other.